EXPERIMENTAL VALIDATION OF THE AZIMUTHAL HIGH FREQUENCY CUTOFF OF HIGH RESOLUTION SATELLITE RADAR IMAGES OF THE OCEAN

MICHAEL ROBINSON, MATTHEW HUBLER, MARK VERDI

Abstract. High resolution synthetic aperture radar (SAR) images of the ocean could be used to improve maritime weather reporting and prediction by detecting small spatial and temporal wind features. In addition to modulation caused by the shape of ocean waves, SAR images are sensitive to nonlinear distortion due to Doppler effects induced by ocean wave motion. The largest effect of this distortion is a sharp spatial high frequency cutoff in the azimuthal direction. This article presents (1) a controlled experimental validation of the azimuthal cutoff and its effects on imagery, and (2) observations of gusts tens of meters across in high-resolution spaceborne SAR images. Various models of the azimuthal cutoff have been proposed and tested on low resolution platforms, but they have not been tested on high resolution, satellite-borne platforms. This article presents an experimental analysis of the azimuthal cutoff in high-resolution images, and shows that the azimuthal cutoff is not necessarily the dominant cause of azimuthal blurring. We show that wind speed appears to be a more important factor, so sometimes the blurring is much less than the azimuthal cutoff suggests. As evidence of this, we exhibit imagery showing subtle changes on the ocean surface due to up- and down-welling solitons.

1. Introduction

Predictive models of the weather rely on accurate wind estimates [1]. It is well known that the predictions given by weather models are highly sensitive to errors in the input wind measurements. (One of the best-known examples of chaos, the Lorenz system, was discovered in a simplified weather model.) The errors due to low resolution measurements can significantly impact the inferences one makes from these models, especially if they are used for providing long-term climatological insight [26].

Remote measurement of ocean winds is usually performed using a device called a *scatterometer*. Unfortunately, persistent satellite-borne scatterometer systems suffer from low spatial and temporal resolution. They provide measurements spaced kilometers apart and additionally require two coincident collections for each measurement. Since these two collections are taken from different portions of the orbit, a given measurement incorporates two separate observations that are minutes apart (or longer). Therefore, quickly changing phenomena cannot be measured, especially if they are physically small. A small or fleeting wind feature (a *gust*) can dissipate or move over the time interval between these collections.

To reduce the effect of ocean surface motion over the course of the data acquisition, we focus on the analysis of a single high resolution synthetic aperture radar (SAR) collection, so the acquisition time is about 7 seconds or less. We successfully

measured quickly changing phenomena whose physical scale was smaller – on the order of tens of meters.

In addition to modulation caused by the shape of ocean waves, SAR images are sensitive to nonlinear distortion due to Doppler effects induced by ocean wave motion. The largest effect of this distortion is a sharp azimuthal *cutoff* – a dramatic reduction of energy – above a certain spatial frequency (wavenumber). This could limit the effective resolution in the azimuthal direction. Various models of the azimuthal cutoff have been proposed and tested on low resolution platforms, but they have not been tested on high resolution, satellite-borne platforms. Using a controlled experimental comparison against oceanographic buoys, this article shows that the model proposed by Hasselmann *et al.* [11] continues to be valid up to 30 cm resolution, which is considerably higher than previous studies. (The ERS wave mode has a resolution of 65.8 m, for instance [2].)

Since the azimuthal cutoff reduces resolution in the azimuthal direction, it could impede the detection of subtle changes in the ocean surface due to gusting. Using typical azimuthal cutoff values (about 0.05 rad/m, see for instance Figure 3), the azimuthal resolution of an ocean SAR image could be limited to about 100 m. We exhibit 30 cm resolution images with a little less than this amount of azimuthal blurring. This is somewhat pessimistic – in another image with a similar azimuthal cutoff, the azimuthal resolution is sufficient to resolve much smaller wind-driven features. That image (see Figure 6) includes a striking example of what appears to be the result of vertical motion of the air column near the ocean surface. Vertically-moving, isolated waves or *solitons* in the air column leave a distinctive impression on a SAR image (see for instance [17]) and alter the local spectra as we describe.

1.1. **Historical context.** The use of two dimensional local spectra to extract wave direction from spaceborne SAR images was initially pioneered by Gerling [9] using SEASAT. Hasselmann and Hasselmann [11] quantified some of the nonlinear effects induced on local spectra by motion, which lead to a spectral inversion algorithm. Their derivation was simplified by Krogstad [16]. Extracting the ocean height and slope spectra from SAR images using a variety of spectral inversion algorithms followed in the work of many other authors, and using several platforms including ERS-1/2 and RadarSat [14, 21, 8, 7, 25].

Extracting wave direction from two dimensional spectra has good support in the literature, including several studies that fused SAR imagery with buoys to obtain more accurate results [28, 12]. The success of recent studies using the ERS-1/2 and ENVISAT wave mode [4, 13] suggest that improved SAR resolution can result in reliable, high-resolution wave measurements. Collard [4] used the ENVISAT wave mode to measure the wave height and direction. They found good agreement between wave spectra derived from SAR and *in situ* measurements. Additionally, several recent studies [5, 20, 3] used TerraSAR-X imagery to great effect.

Additionally, SAR images are sensitive to texture at smaller spatial scales than are scatterometers. This makes them ideal for detecting complex weather features over the ocean. This has been known for some time – for instance Mourad [22] used SEASAT to examine dynamics of cold air masses. Later studies using RadarSat [27, 17, 18] and ENVISAT [19] have shown that high-resolution SAR can be extremely effective at detecting and examining turbulent wind behaviors over the ocean.

1.2. **Contributions.** This article makes two substantive contributions, namely (1) a controlled experimental validation of the azimuthal cutoff described in [11] at considerably higher resolution than has been done before and (2) the first reported observation of a downwelling soliton (a "downdraft") in a SAR image and its subsequent local spectral analysis. We show that azimuthal cutoff and azimuthal blurring are probably caused by two related (but different) wind-driven effects. Based on this spectral analysis, we hypothesize that changes in wind-driven surface texture coincide with substantial structural changes in spectrum in addition to variations in reflectivity.

2. Experimental design

Moving objects in a SAR image are displaced from their true position along the azimuthal direction. If an object in motion is coming towards the satellite parallel to its look direction, the its echo appears shifted in the azimuthal direction (the same direction as the flight path). The reverse occurs if the object is in motion away from the satellite – the echo shifts in the opposite direction of the flight path. The azimuthal displacement applies an additional modulation to ocean waves in the azimuthal direction. The modulation causes evenly-spaced waves to appear "bunched" into groups, which obscures the high frequency content in the azimuthal direction. As discussed in Collard [4] and many others, the dominant effect of this bunching is manifested as a high spatial frequency cutoff applied to the spectrum in the azimuthal direction.

Various observations and empirical formulas for the azimuthal cutoff have been proposed, for instance Gaussian cutoff. This was shown theoretically in [11, Eq. (56)], which presented a systematic asymptotic derivation of the dimensionless azimuthal cutoff factor

$$\exp(-k_x^2 E[\xi^2]), \tag{1}$$

in which k_x is the azimuthal wavenumber (radians per meter) and $E[\xi^2]$ is the mean squared azimuthal displacement (meters). They tested this formula extensively against SEASAT imagery and found good numerical agreement in about half of the cases they tried. Subsequently Collard [4] also indicated that a Gaussian cutoff appears to match the data well, but did not conduct an extensive comparison against *in situ* measurements. Our experimental procedure aims to validate (1) by comparing spectra derived from SAR images against spectra derived from buoys.

We employed the German satellite TerraSAR-X as a SAR imagery source. This platform provides high resolution, polarimetric radar images at 9.6 GHz. We acquired 5 images (see Table 1 and Figure 1) centered near 4 buoy locations (see Table 2). The Portland single and Portland dual images were taken from the vicinity of the same buoy. "Single" and "dual" refer to the acquired polarizations. Since the buoys record wind speed and direction hourly, Table 2 also shows the wind measurements nearest to the imaging time. We selected these specific buoys because they acquire wave spectrum data (see Figure 2) in addition to wind measurements.

3. Spectral width validation

We processed the satellite and the buoy measurements independently to provide validation of the azimuthal cutoff formula. Specifically, we used the collection geometry and the buoy's measurement of the ocean spectrum during the collection

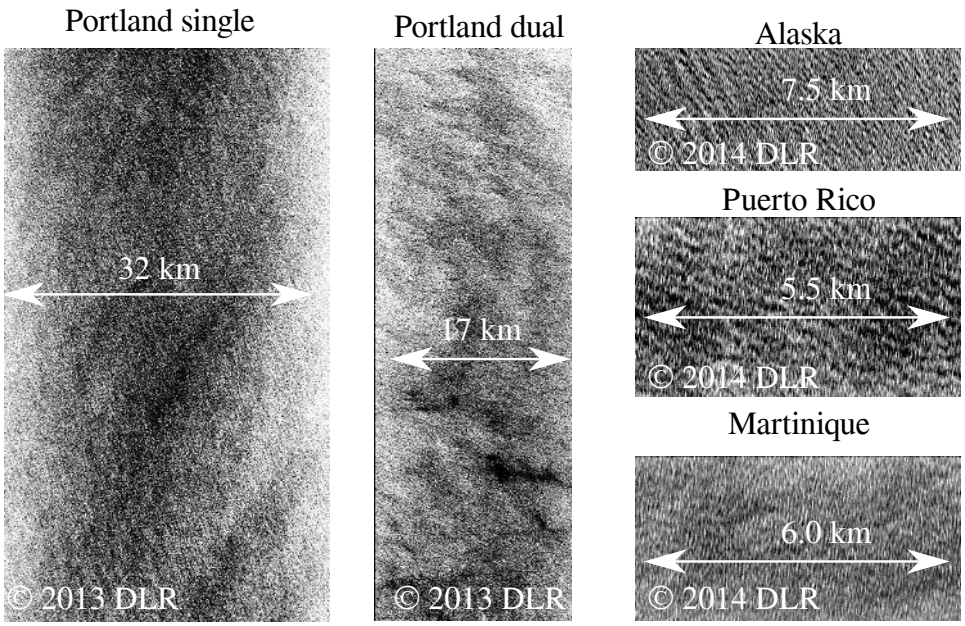

FIGURE 1. Low-resolution snapshots of each image that was collected. In all images, the horizontal axis is the range direction, and the vertical direction is the azimuthal direction. (See also Table 1)

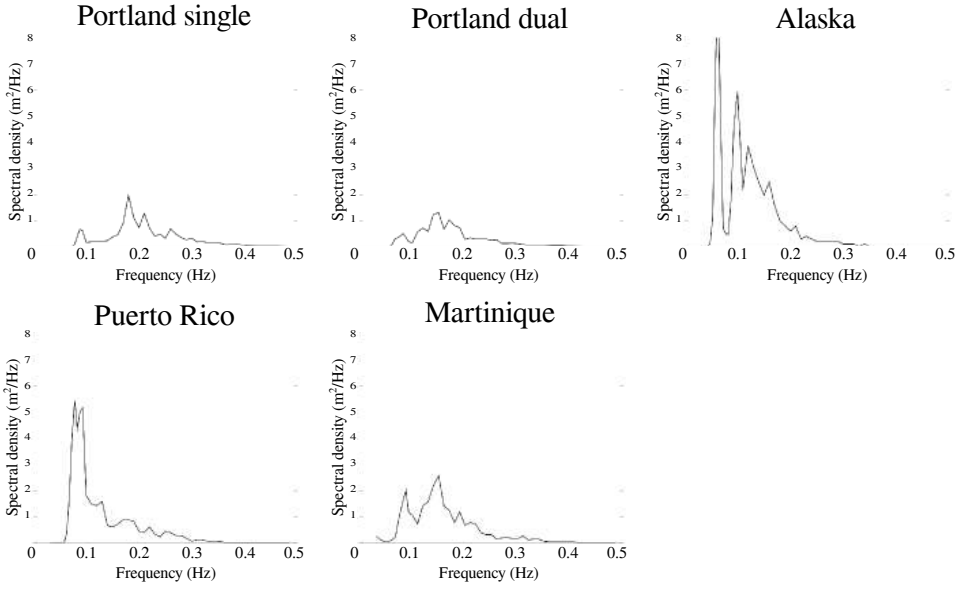

FIGURE 2. Wave height power spectral density as measured by the buoys coincident with each image

TABLE 1. Overview of data collections

Image name	Date	Center Lat	Center Lon	Pol	Res
Portland single	2013-4-24	45.969° N	125.725° W	HH	1.25 m
Portland dual	2013-4-28	46.009° N	125.630° W	HH,VV	2.75 m
Alaska	2014-4-04	52.785° N	155.045° W	VV	0.32 m
Puerto Rico	2014-4-05	21.062° N	64.965° W	HH	0.26 m
Martinique	2014-4-09	14.330° N	46.079° W	HH	0.24 m

TABLE 2. Overview of buoys and their measurements

Image name	NOAA ID	Latitude	Longitude	Wind speed	Wind dir
Portland single	46089	45.893° N	125.819° W	3.7 m/s	254° N
Portland dual	46089	45.893° N	125.819° W	3.7 m/s	262° N
Alaska	46066	52.785° N	155.047° W	10.4 m/s	272° N
Puerto Rico	41043	21.061° N	64.966° W	9.1 m/s	16° N
Martinique	41041	14.329° N	46.082° W	9.7 m/s	57° N

to predict the azimuthal cutoff that should be visible in a typical SAR image, against which we compared the actual azimuthal cutoff.

The buoy-derived power spectral density associated to the ocean surface height distribution nearest to the time of each collection is shown in Figure 2. (Each buoy reports a spectrum hourly.) Assuming the buoy power spectral density $\Phi(f)$ is a known function of frequency f, the mean squared height displacement is given by (see [15, 7.3:21])

$$E[h^2] = \frac{1}{2\pi} \int \Phi(f)\, df. \tag{2}$$

From this, the mean orbital velocity of a particle on the ocean surface is given by (see [15, 3.3:8.1] or [11, (44)-(45)])

$$E[v^2] = \int f\, \Phi(f)\, df. \tag{3}$$

The SAR collection geometry with respect to the wind speed induces a linear modulation according to the component of the velocity projected onto the range direction [11, (17)]. The projected mean squared velocity is $E[w^2]$, given by

$$E[w^2] = E[v^2] \left(\cos^2 \phi \sin^2 \theta + \cos^2 \theta \right), \tag{4}$$

where ϕ is the difference between the wind and look direction angles and θ is the incidence angle. The first term in (4) corresponds to modulation of the look direction component of the orbital velocity, while the second term corresponds to modulation of the vertical component of the orbital velocity. With the projected mean squared velocity $E[w^2]$ in hand, the mean squared azimuthal displacement $E[\xi^2]$ can be computed via

$$E[\xi^2] = \frac{R^2}{U^2} E[w^2], \tag{5}$$

where R is the slant range and U is the platform velocity (assuming no crabbing). Upon substitution into (1), this results in a half-power (3 dB) azimuthal cutoff k_x

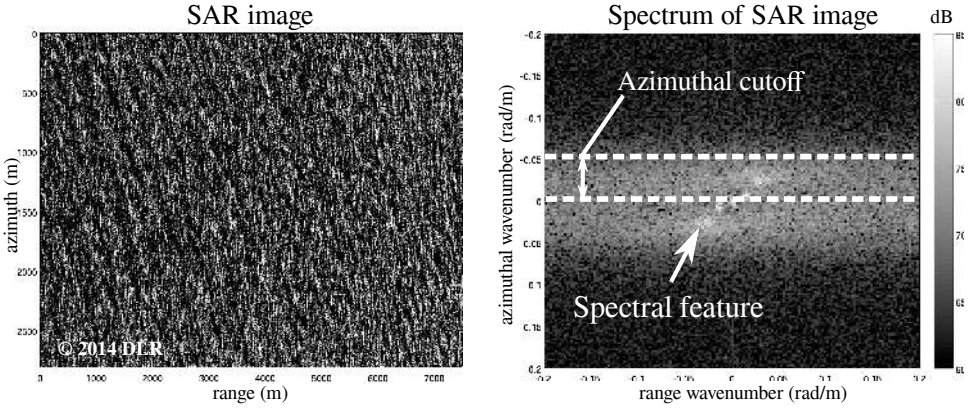

FIGURE 3. Alaska VV SAR image (left) and its spectrum (right), showing the 3 dB azimuthal cutoff

estimate

$$k_x = \sqrt{\frac{\ln 2}{E[\xi^2]}}, \tag{6}$$

which we estimate visually from SAR images.

For each image collected, we measured the 3 dB spectral width about the zero azimuthal wavenumber. For instance, Figure 3 shows the azimuthal cutoff in the Alaska VV image.

Cuts of the spectrum along the azimuthal direction (about 0.05 rad/m away from the origin) for each image are shown in Figure 4. It is apparent that each spectral plot is approximately Gaussian, in agreement with [4]. Each spectrum is normalized, and a dotted line 3 dB below the peak is shown on each image to aid in comparison with (6).

All of the relevant buoy measurements are shown in Table 3. Some of the entries in Table 3 are derived from Figure 2 and Table 2. Table 3 also shows the measured azimuthal cutoffs from each image (the intersection of the 3 dB lines with the measurements in Figure 4). Each spectrum is not exactly symmetric, so in each case we selected the larger of the two width measurements.

Since we measured the image-derived azimuthal cutoff values manually, they are at best accurate to about $\pm$ 3 samples, which is mostly due to noise levels in the image. At the highest resolution, we computed the spectrum of a 8000×8000 pixel subimage, which at 0.32 m/pixel, yields an error about 0.0025 rad/m per pixel. This is about $\pm 15\%$. Of our five images, four fall within this experimental error level, and one image is outside (but very close to) the level of experimental error. Without additional data – five images is insufficient to draw a statistically significant conclusion – it is difficult to explain why the Martinique spectral cutoff value lies outside the experimental error. However, we speculate that polarization plays an important role in accurate spectral measurements. Although TerraSAR-X was unable to obtain both polarizations for the Alaska, Puerto Rico, and Martinique images, we note that the VV-polarized Alaska image performed considerably better

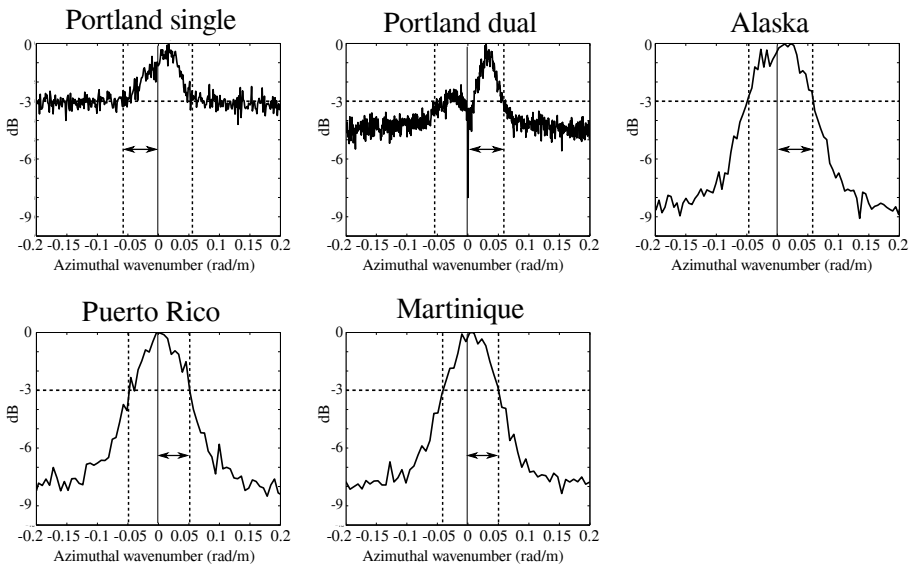

FIGURE 4. Azimuthal spectrum for each image. The 3 dB cutoff is shown as a dotted line in each frame. The larger of the two widths (used in Table 3) is marked by an arrow.

TABLE 3. Summary of azimuthal cutoff calculations

Parameter	Source	Portland single	Portland dual	Alaska	Puerto Rico	Martinique	Units
Resolution	DLR	1.25	2.75	0.32	0.26	0.24	m
Acq. time	DLR	8	7	1	1	1	s
Polarization	DLR	HH	VV	VV	HH	HH	
Spectral peak	Fig. 2	0.13	0.09	0.016	0.024	0.090	rad/m
Wind direction	Buoy	350°	262°	272°	16°	57°	deg true N
Wind speed	Buoy	3.7	3.7	10.4	9.1	9.7	m/s
RMS displacement	Eq. (2)	0.15	0.14	0.27	0.21	0.19	m
RMS orbital velocity	Eq. (3)	0.21	0.16	0.22	0.19	0.20	m/s
Slant range	DLR	796	700	574	600	616	km
Satellite speed	DLR	7.7	7.7	7.7	7.7	7.7	km/s
Incidence angle	DLR	44°	42°	25°	34°	37°	deg from vert
Look direction	DLR	279°	81°	282°	80°	79°	deg true N
Az. displacement	Eq. (5)	15.5	14.3	18.4	16.3	15.5	m
Az. cutoff	Eq. (6)	0.053	0.058	0.056	0.059	0.060	rad/m
Az. cutoff	Fig. 4	0.055	0.061	0.056	0.051	0.049	rad/m
Percent error		-2.3%	-5%	0%	14%	22%	

than the HH-polarized Puerto Rico and Martinique images. Further study is needed to discern the role of polarization at this high resolution.

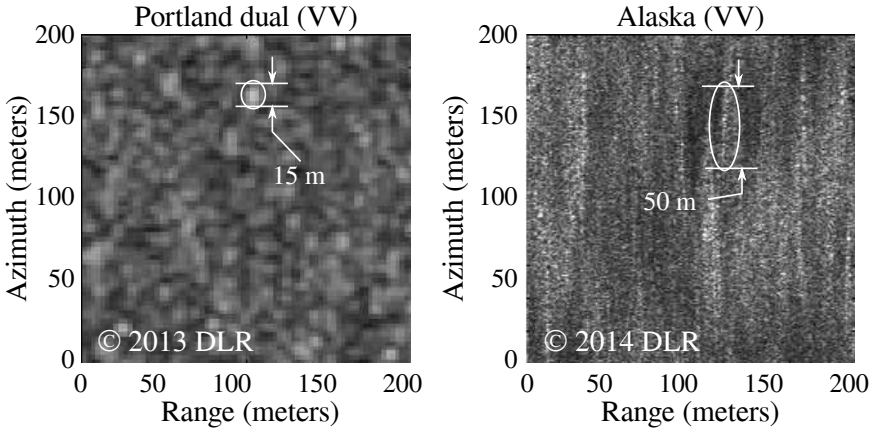

FIGURE 5. Portions of the Portland dual (left) and Alaska (right) images. Substantial azimuthal blurring is visible in the Alaska image.

4. Small-scale spatial and spectral details

An azimuthal cutoff of approximately 0.05 rad/m means that all waves of wavelength less than $2\pi/0.05 = 100$ m could be hard to resolve. Surprisingly, all of our images seem to have better azimuthal resolution than this, though substantial azimuthal blurring is visible in the Alaska, Puerto Rico, and Martinique images. Azimuthal blurring is not visible in either of the Portland images. Figure 5 shows a comparison of two typical subimages taken from the Portland dual and Alaska images. Both subimages are shown with the same spatial scale even though they were taken with different resolutions, which accounts for the difference in spatial discretizations.

Even though the Portland dual and Alaska images have approximately the same azimuthal cutoff (see Table 3), there is a substantial difference in wind speed, but *not* orbital velocity. Because of this, we conclude that the azimuthal blurring in the Alaska image can be attributed to a wind-driven effect. To see this, let us estimate the effective resolution of the image by considering the spatial size of a localized bright spot (a specular "flash") within the SAR image. As shown in Figure 5, a typical specular flash in the Portland dual image has azimuthal size 15 m, while in the Alaska image it is 50 m. (The reader is cautioned that there are many more specular flashes in the Alaska image. Flashes can overlap, which can give a misleadingly high blurring length. The flash which is marked in Figure 5 doesn't overlap any others.) The ratio between these two specular flash sizes is 0.3 – within 15% of the ratio of wind speeds, which is 0.35. (See Table 2 for the wind speeds, namely 3.7 m/s in the Portland dual image and 10.4 m/s in the Alaska image. Also notice that the image-to-image difference in wind direction with respect to the satellite flight path is within about 10°, so the collection geometries are comparable.)

The velocity corresponding to an azimuthal displacement of 15 m in the Portland image is 0.16 m/s, which matches the orbital velocity in Table 3 closely. On the other hand, an azimuthal displacement of 50 m in the Alaska image is 0.67 m/s,

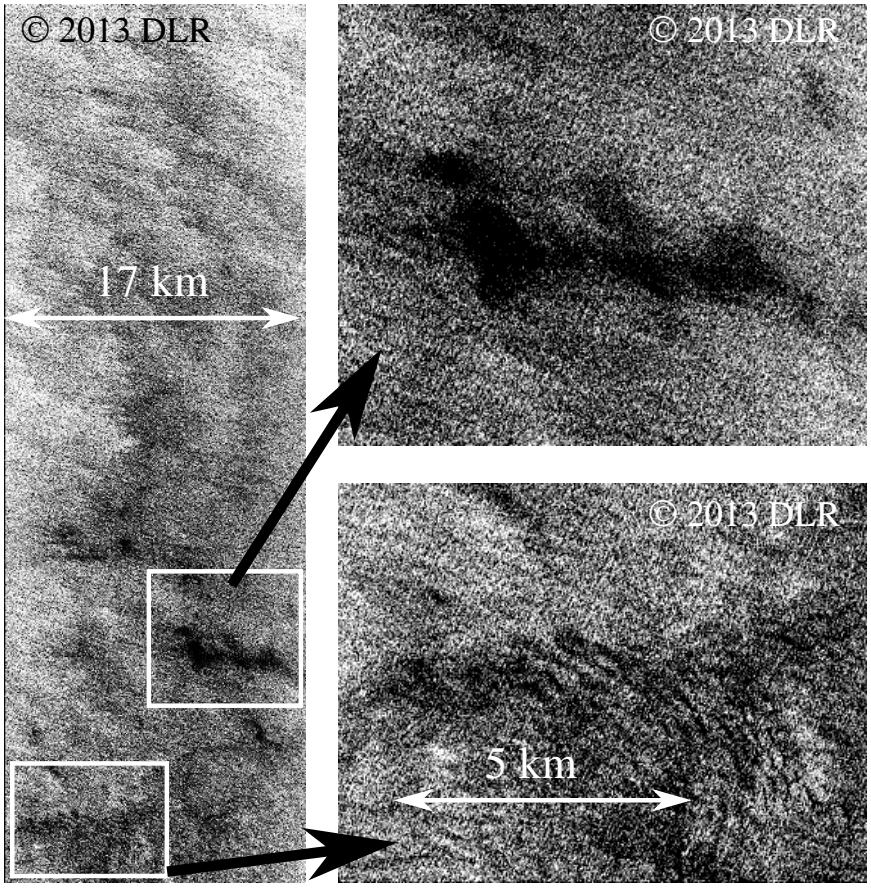

FIGURE 6. The VV polarization of the Portland dual image (left) and two locations of interest zoomed (right)

which exceeds the orbital velocity by a factor of 3. This likely indicates a discrepancy between short fetch (azimuthal blurring) and long fetch (azimuthal cutoff) waves, although additional images should be collected and analyzed to reinforce this hypothesis.

Even with substantial azimuthal blurring in the Alaska image, it is still possible to discern detail in the spectral features as shown at right in Figure 3. Although we do not have data corresponding to the specific features we observed, our preliminary analysis indicates that there is considerable detail in ocean surface texture that is visible even when the azimuthal cutoff is small. We believe that differences in texture correspond to local variations in wind and surface current.

Given our hypothesis that azimuthal blurring is reduced by lower wind speeds, it is not surprising that the Portland images exhibit complicated surface structure. Figure 6 shows the Portland dual image, in which there are two areas we investigated further: a set of concentric "rings" in the bottom-left corner of the image and a prominent "dark spot" in the lower-middle portion of the image. Comparison with the images acquired by Li and their discussion in [17] suggests that the dark spot

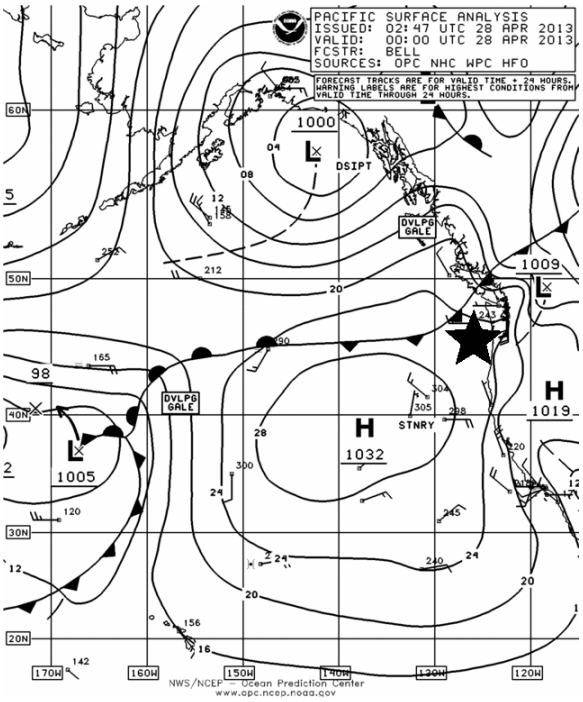

FIGURE 7. NOAA maritime surface analysis closest to the time of the Portland dual image [23]. The star indicates the scene location.

most likely indicates the presence of an upwelling soliton. The NOAA maritime surface analysis near the imaging time (Figure 7) indicates that a front is near the scene, which may be the cause of turbulence in the area. Because of its proximity to the upwelling, we suspect that the concentric rings in the bottom-left corner of the image correspond to ocean waves radiating away from an atmospheric downdraft.

Figure 8 shows the spectra within these features, as well as the spectrum of a "normal" patch of ocean. As one might have guessed, the spectral features seem to die out over the dark region, which suggests that the speed of the wind tangent to the surface has decreased consistent with an upwelling. Compared to the "normal" image, we see that the high spectral values almost completely dissipate. Over the downdraft, the spectrum disperses somewhat, possibly indicating an unstable wind direction.

5. Conclusions

We have shown that the formula for azimuthal cutoff derived by Hasselmann [11] appears to be valid for high resolution SAR images of the ocean surface. The expected spectral shape of a SAR image of the ocean is Gaussian in the azimuthal direction. VV polarized images may result in a closer agreement with theory. Although the azimuthal cutoff does degrade azimuthal resolution, it does not completely obscure the visibility of wind-driven spectral features, and the effective azimuthal resolution is still sufficient to detect features tens of meters across. Azimuthal blurring appears to be driven primarily by wind speed even though the

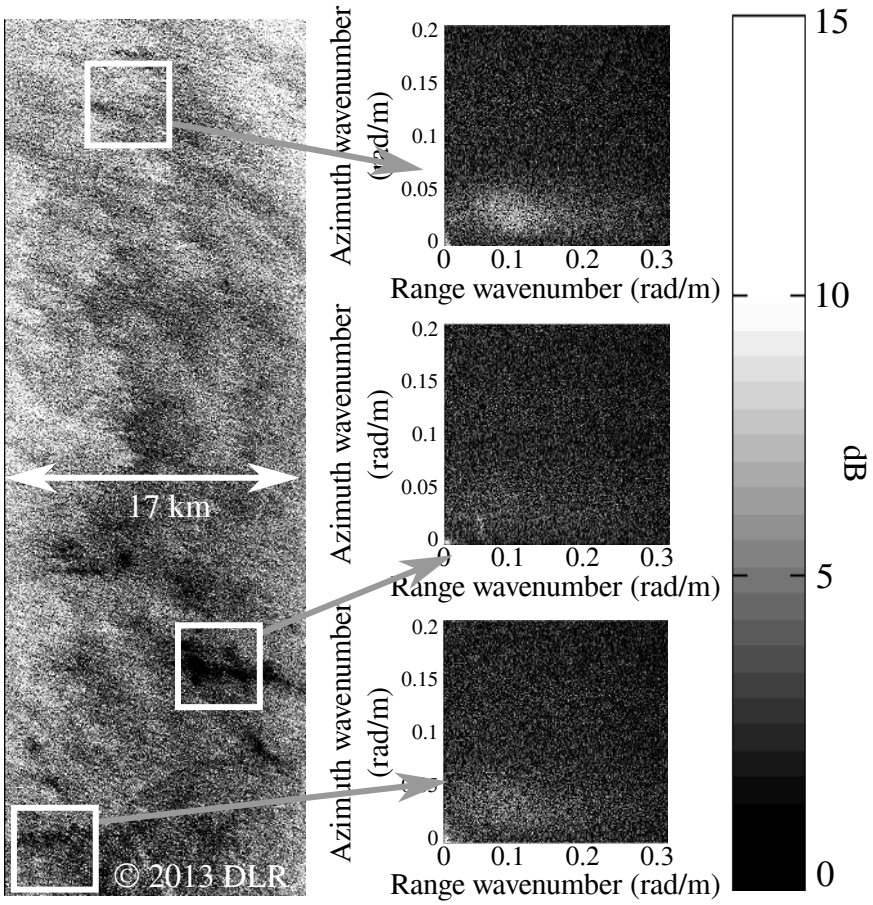

FIGURE 8. The VV polarization of the Portland dual image (left) and spectra measured at several locations of interest (right)

azimuthal cutoff is an effect of wave orbital velocity. This explains why we were able to detect the presence of an downdraft over the ocean when the wind is calm. Under the appropriate wind conditions, high resolution SAR images of the ocean therefore offer the ability to make accurate measurements of gusts that are only tens of meters across.

ACKNOWLEDGMENTS

The authors acknowledge financial support from the Faculty Research Support Grant at American University, Federal Contract FA9550-09-1-0643, and the DC Space Grant Consortium. The authors also thank the Deutsches Zentrum für Luft und Raumfahrt (DLR) for supplying the data used on this project.

REFERENCES

[1] Joan Ulrich Von Ahn. The impact of QuikSCAT winds on the issuance of marine wind warnings. *Mariners' Weather Log*, 47(2), December 2003.

[2] Guy Brooker. UWA processing algorithm specification. Technical Report ER-TN-ESA-GS-0342, European Space Agency, 1995.
[3] Miguel Bruck and Susanne Lehner. Coastal wave field extraction using TerraSAR-X data. *Journal of Applied Remote Sensing*, 7(1):073694–073694, 2013.
[4] Fabrice Collard, Fabrice Ardhuin, and Bertrand Chapron. Extraction of coastal ocean wave fields from SAR images. *Oceanic Engineering, IEEE Journal of*, 30(3):526–533, 2005.
[5] Guillermo M Diaz Mendez, Susanne Lehner, Francisco J Ocampo-Torres, Xiao Ming Li, and Stephan Brusch. Wind and wave observations off the south Pacific coast of Mexico using TerraSAR-X imagery. *International Journal of Remote Sensing*, 31(17-18):4933–4955, 2010.
[6] P. DiGiacomo, L. Washburn, B. Holt, and B. Jones. Coastal pollution hazard in southern California observed by SAR imagery: stormwater plumes, wastewater plumes, and natural hydrocarbon seeps. *Marine Pollution Bulletin*, 2004.
[7] Michael Dowd, Paris W Vachon, Fred W Dobson, and Richard B Olsen. Ocean wave extraction from RADARSAT synthetic aperture radar inter-look image cross-spectra. *Geoscience and Remote Sensing, IEEE Transactions on*, 39(1):21–37, 2001.
[8] Geir Engen, Paris W Vachon, Harald Johnsen, and Fred W Dobson. Retrieval of ocean wave spectra and RAR MTFs from dual-polarization SAR data. *Geoscience and Remote Sensing, IEEE Transactions on*, 38(1):391–403, 2000.
[9] T. W. Gerling. Structure of the surface wind field from the SEASAT SAR. *J. Geophys. Res.*, 91(C2):2308–2320, 1986.
[10] F. Girard-Ardhuin, G. Mercer, and R. Garello. Oil slick detection by SAR imagery: potential and limitations. In *OCEANS*, 2003.
[11] K. Hasselmann and S. Hasselmann. On the nonlinear mapping of an ocean wave spectrum into a synthetic aperture radar image spectrum and its inversion. *Journal of Geophysical Research*, 96(C6):10713–10729, June 1991.
[12] S Hasselmann, P Lionello, and K Hasselmann. An optimal interpolation scheme for the assimilation of spectral wave data. *Journal of Geophysical Research: Oceans (1978–2012)*, 102(C7):15823–15836, 1997.
[13] Jochen Horstmann and Wolfgang Koch. Measurement of ocean surface winds using synthetic aperture radars. *Oceanic Engineering, IEEE Journal of*, 30(3):508–515, 2005.
[14] Vincent Kerbaol, Bertrand Chapron, and Paris W Vachon. Analysis of ERS-1/2 synthetic aperture radar wave mode imagettes. *Journal of Geophysical Research: Oceans (1978–2012)*, 103(C4):7833–7846, 1998.
[15] B. Kinsman. *Wind waves: their generation and propagation on the ocean surface*. Prentice-Hall, 1965.
[16] Harald E Krogstad. A simple derivation of Hasselmann's nonlinear ocean-synthetic aperture radar transform. *Journal of Geophysical Research: Oceans (1978–2012)*, 97(C2):2421–2425, 1992.
[17] Xiaofeng Li, Changming Dong, Pablo Clemente-Colón, William G Pichel, and Karen S Friedman. Synthetic aperture radar observation of the sea surface imprints of upstream atmospheric solitons generated by flow impeded by an island. *Journal of Geophysical Research: Oceans (1978–2012)*, 109(C2), 2004.
[18] Xiaofeng Li, Weizhong Zheng, William G Pichel, Cheng-Zhi Zou, and Pablo Clemente-Colón. Coastal katabatic winds imaged by SAR. *Geophysical research letters*, 34(3), 2007.
[19] Xiaofeng Li, Weizhong Zheng, Xiaofeng Yang, Jun A Zhang, William G Pichel, and Ziwei Li. Coexistence of atmospheric gravity waves and boundary layer rolls observed by SAR. *Journal of the Atmospheric Sciences*, 70(11):3448–3459, 2013.
[20] Xiaoming Li, Susanne Lehner, and Wolfgang Rosenthal. Investigation of ocean surface wave refraction using TerraSAR-X data. *Geoscience and Remote Sensing, IEEE Transactions on*, 48(2):830–840, 2010.
[21] C Mastenbroek and CF de Valk. A semiparametric algorithm to retrieve ocean wave spectra from synthetic aperture radar. *Journal of Geophysical Research: Oceans (1978–2012)*, 105(C2):3497–3516, 2000.
[22] Pierre D Mourad and Bernard A Walter. Viewing a cold air outbreak using satellite-based synthetic aperture radar and advanced very high resolution radiometer imagery. *Journal of Geophysical Research: Oceans (1978–2012)*, 101(C7):16391–16400, 1996.
[23] NOAA. Pacific east surface analysis. http://nomads.ncdc.noaa.gov/ncep-charts/hires/20130428/pace.sfcanal.00.2013042802.gif, 2013.

[24] M. Rey. Application of Radon transform techniques to a wake detection in SEASAT. *IEEE Geosciences and Remote Sensing*, 1990.
[25] J Schulz-Stellenfleth, S Lehner, and D Hoja. A parametric scheme for the retrieval of two-dimensional ocean wave spectra from synthetic aperture radar look cross spectra. *Journal of Geophysical Research: Oceans (1978–2012)*, 110(C5), 2005.
[26] S. Strogatz. *Nonlinear Dynamics And Chaos*. Perseus, 2008.
[27] Donald R Thompson and Robert C Beal. Mapping high-resolution wind fields using synthetic aperture radar. *Johns Hopkins APL Technical Digest*, 21(1):58–67, 2000.
[28] AC Voorrips, VK Makin, and S Hasselmann. Assimilation of wave spectra from pitch-and-roll buoys in a north sea wave model. *Journal of Geophysical Research: Oceans (1978–2012)*, 102(C3):5829–5849, 1997.

Department of Mathematics and Statistics, American University, 4400 Massachusetts Ave NW, Washington, DC 20016